SCIENTIFIC PAPER

APPLICATION OF WASTE RAW MATERIALS AS A REINFORCEMENT FOR PROTECTIVE COATINGS BASED ON PYROPHYLLITE

Marko Pavlović[1], Marina Dojčinović[2], Jasmina Nikolić[2], Anja Terzić[3], Vladimir Pavićević[2], Saša Drmanić[2*], Enita Kurtanović[4]

[1]Innovation Center of Faculty of Mechanical Engineering, University of Belgrade, Kraljice Marije 16, 11000 Belgrade, Serbia

[2]Faculty of Technology and Metallurgy, University of Belgrade, Karnegijeva 4, 11000 Belgrade, Serbia

[3]Institute for Testing of Materials, Bulevar vojvode Mišića 43, 11000 Belgrade, Serbia

[4]AD HARBI, Tvornička 3, 71210 Ilidža/Sarajevo, B&H

https://doi.org/10.2298/CICEQ240410029P

Received 10.4.2024.

Revised 18.6.2024.

Accepted 17.7.2024.

* Correspondence: prof dr Saša Drmanić; e-mail drmana@tmf.bg.ac.rs; Phone no: 011/3303669; Fax: 3370387

Abstract

In this study, pyrophyllite was used for the first time in the composition of protective refractory coatings together with supplementary waste resources. The proposed refractory coatings are applicable for metallic and non-metallic structures, with the option of using them to protect machinery components in the chemical industry, metallurgy, and mining. Given that pyrophyllite has a low hardness, the goal was to improve the coating's resistance to cavitation erosion by adding 20 wt.% of hard refractory materials, i.e., crushed and micronized waste bricks based on mullite and corundum, respectively. Previous studies have demonstrated that protective coatings using a pyrophyllite filler have refractory qualities but insufficient resistance to cavitation erosion. As a result, the composition of refractory coatings, the preparation techniques, and the coating manufacturing process were altered. This study presents a simple method for combining conventional coatings made of refractory fillers (primary resource: pyrophyllite) with waste materials (mullite brick and corundum brick) used as reinforcement in protective refractory coatings for metal and non-metal structural elements that are highly resistant to cavitation erosion.

Keywords: construction materials; waste resources; metal substrate; microstructure; cavitation erosion.

Article Highlights

- Pyrophyllite was used as an 80% filler in protective coatings, with 15% silicone resin acting as a binder.
- 20% of secondary raw material additions based on mullite and corundum increased the protective coating's durability.
- PM20 and PC20 coatings had cavitation rates of 0.22 mg/min and 0.14 mg/min, respectively, indicating cavitation erosion resistance.

INTRODUCTION

Chemical, mechanical, and construction industry professionals are looking for innovative building materials that have the potential to reduce energy consumption, increase thermal insulation, and minimize CO_2 emissions. The world is today facing major energy issues and concerns as a result of rising living standards and rapid population expansion. Industry (chemical, machine, building, etc.) is one of the primary sectors recognized for having a large impact on atmospheric carbon dioxide emissions, which contribute to global warming [1, 2]. The primary goal is to identify new solutions to reduce CO_2 emissions in the industry sector through innovative use of alternative raw materials [3-5]. The industry's aim is to use raw materials from waste streams, which are resources that correspond to the Green Agenda principles [6, 7]. In this experiment, discarded mullite and corundum bricks were used as an alternative raw material for reinforcement in refractory coatings.

Pyrophyllite was used in this work as the base material for producing the refractory coatings. The main characteristic of this mineral is that it is composed of two tetrahedral Si sheets placed between an Al octahedral sheet to form a layered hydroxy-aluminosilicate [8]. In octahedral form, every Al atom of pyrophyllite has four O atoms connected to Si tetrahedra. Two structural OH groups are also bound to Al atoms [9]. Pyrophyllite is characterized by its unique crystalline structure and softness of talc [10]. Due to the specific structure and the O atoms placement between the layer surfaces, pyrophyllite is extremely resistant to acids, which is important when this mineral is employed in design of coatings [11, 12]. The typical impurities found in pyrophyllite usually include mica, bauxite, diaspore, and quartz. When heated, pyrophyllite loses the structural OH groups linked to its octahedral sheet (550°C) and creates mullite and cristobalite (1200°C), which are refractory mineral phases [13-15]. Pyrophyllite's main uses are in the refractory and ceramic industries, which are established by its excellent heat resistance, stable crystal structure during heating, and consistent chemical composition [16].

The resistance of substate to different types of erosion (such as carbonation, chloride ion erosion, and cavitation erosion via water) can be greatly increased by application of the organic-based coatings to metal or non-metal (e.g., concrete) surfaces [17–20]. Several studies have demonstrated that the most crucial elements for establishing a protective layer on the surface of a material are the organic film-forming coatings of high density and stable chemical composition [21, 22]. This layer keeps metal or non-metal components inside a structure safe from corrosive

environmental media (heat, moisture, and acids) [23]. Protective coatings have become more and more important as an auxiliary technology to ensure the long-term service performance of metal, concrete, and/or composite structures in residential and commercial settings [24, 25]. The basic idea is to produce a relatively non-toxic, extremely erosion-resistant, and easily clean protective coating using water as the dispersing medium, a low organic content, and an inorganic raw material (filler) with a high hardness value and good grain size and shape distribution.

This study presents an easy approach to transform traditional coatings formed of refractory filler (primary resource: pyrophyllite) with waste materials (pulverized mullite brick and corundum brick) used as reinforcement in protective refractory coatings for metal and concrete structural elements that are resistant to cavitation erosion.

EXPERIMENTAL

Materials and mix-design of the coatings

Pyrophyllite (mineral formula: $Al_2Si_4O_{10}\cdot(OH)_4$) was used as a base material in the mix design of experimental coatings. Since the pyrophyllite mineral belongs to the talc group, the performance and characteristics of pyrophyllite are similar to those of talc. Namely, pyrophyllite has a hardness of 1-2 on the Moh's scale of hardness, which is very low. Thereby, the addition of certain “reinforcing” raw materials is necessary to improve the coatings’ hardness and mechanical characteristics.

Pyrophyllite ore was extracted from the Parsovići deposit, located in Bosnia and Herzegovina. The usual ore sampling campaign was carried out in order to prepare a representative 300-kilogram sample [26]. The original pyrophyllite ore was quartered and roughly crushed using a cone and jaw crushers to break the ore crude mass up into 10 kg sub-samples. After rough crushing, the subsamples (10 kg) were further milled and finally pulverized in an ultra-centrifugal mill. Pyrophyllite sub-samples were subjected to wet sieving on a series of W.S. Tyler test sieves in order to analyze the particle sizes (Figure 1). The average grain size of the pyrophyllite grain mixture was d50 =20μm. The mean grain shape factor was 0.67 (semi-round) [27, 28]. The pyrophyllite mineral was found to be the dominant phase, accounting for up to 50% of all current crystalline phases, according to an X-ray diffraction examination of the pyrophyllite sample (Figure 2). In the analyzed sample, the amounts of quartz, calcite, and

dolomite were less abundant, accounting for up to 30%, 10%, and 5%, respectively. Kaolinite was detected in very small amounts [29].

Figure 1.

Figure 2.

Mullite-based material (mullite mineral formula: $3Al_2O_3 \cdot 2SiO_2$) was used as a reinforcement in the mix design of the coating. In order to achieve low-cost coatings, mullite was not synthesized; instead, recycled mullite refractory bricks were employed (acquired from a local refractory construction firm). According to the Rongsheng Kiln Refractory Bricks Manufacturer, mullite is used as the primary raw material for the production of mullite bricks, which are then manufactured *via* molding and high-temperature sintering. The refractoriness of this material is as high as 1600 °C. Bulk density is 1.5 g/cm^3. The cold crushing strength is 9 MPa. The apparent initial softening temperature is 1600°C (conditions: 0.1 MPa, 0.6%). The thermal conductivity is 0.6 W/(m·K). The maximum service temperature is 1550 °C. The samples were crushed and milled to the average d50=15µm. The mean grain shape factor was 0.57 (semi-angular).

Similarly, corundum bricks (corundum mineral formula: Al_2O_3) from the same manufacturer and local distributor were used as refractory reinforcement in the coatingsmix design. The refractoriness of this material is approximately 1800 °C. Bulk density is 2.5 g/cm^3. The cold crushing strength is 25 MPa. The apparent initial softening temperature is 1700 °C (conditions: 0.1 MPa, 0.6%). The thermal conductivity is 0.5 W/(m·K). The maximum service temperature is 1700–1750 °C. The samples were also crushed and milled to the average d50=15µm. The mean grain shape factor was 0.53 (semi-angular).

Cordierite and mullite were also submitted to the sieve analysis to detect the grain-size distribution of these two employed raw materials (Figure 1). Based on data on grain shape [28, 30, 31], i.e., pyrophyllite being semi-round while mullite and corundum being semi-angular, this mix composition is suitable for achieving a good alignment of the grains with each other during coating application, which will contribute to its hardness and adhesion and ultimately better surface protection.

The chemical composition of the raw materials was determined by means of atomic absorption spectrometry on a Perkin Elmer Analyst 300 instrument. Characteristics of the device: wavelength range: 185–900 nm; optical dual beam; monochromator with 1800 lines/mm; photo

multiplicator detector; carrier with 6 lamps with automatic positioning; flame technique; titanium burners of 10 and 5 cm; automatic gas flow adjustment. The chemical composition is provided in Table 1.

Table 1.

Two coatings were prepared for the experiment. The samples were labeled as PM20 and PC20. Both coatings contained pyrophyllite at 80 wt.% in the mix design of filler for coating. The recycled mullite brick was added to PM20 in 20 wt. % (of the total filler mixture mass). Similarly, the recycled corundum brick was added (20 wt.%) to PC20. Dry powders were additionally homogenized in a laboratory mixer (at ambient temperature: 20°C) prior to adding liquid compounds. Siloxane resin with epoxy modification, in liquid form (purchased from manufacturer Evonik Operations GmbH), was added in 15 wt.%. According to the data sheet, SILIKOPON® EF treats successfully at ambient temperature in combination with aminosilanes. Dynasylan® AMEO is an aminosilane-based coupling agent (3.5 wt.%). The ratio between epoxy resin and coupling agent was 4.5:1. Titanium dioxide (TiO_2) (Fisher Chemicals, UK) was used as an additive in the amount of 1.5 wt.% in accordance with the recommendations by the SILIKOPON manufacturer. Mix-design of the experimentally prepared coatings is provided in Table 2.

Table 2.

The powder was initially dissolved in alcohol (ethanol). Then the mixture was added to the siloxane-epoxy resin and mixed for 5 minutes. After adding the coupling agent and additive, the mixture was stirred for an additional 15 minutes. The coatings were spread on the specimens (round steel tin plates of 2 cm diameter) via a film applicator. After the coating process, the specimens were kept at room temperature (20°C) for 24 hours.

Instrumental methods

The experimentally produced PM20 and PC20 refractory coatings were subjected to the standard test procedure for cavitation erosion as per ASTM G32-16 [30,31]. The PM20 and PC20 samples (steel tin coated with experimentally developed coatings) were used in the experiment. The starting masses of the PM20 and PC20 samples were 25 g and 27 g, respectively. The ultrasonic vibratory cavitation method was employed with a stationary sample due to the brittle nature of the examined material. The sample holder was secured to the bottom

of the water bath. The mechanical vibratory concentrator was immersed in a water bath. The water temperature remained constant at 25±1°C. The sample and the front surface of the vibratory concentrator were separated by a 0.5 mm gap. Mechanical vibrations at a frequency of 20 ± 0.2 kHz were employed. Mechanical vibrations at the concentrator top had an amplitude of 50 ± 2 μm. The distance between the test sample and the concentrator was 0.5 mm. A significant cavitation zone developed beneath the concentrator's front surface and the stationary-tested sample. The water bath was cooling the sample to keep it at a constant temperature. A constant water flow formed a pressure field, causing cavitation bubbles to implode on the surface of a sample. The water flow rate was 5-10 ml/s, and the bathroom temperature was 25±1°C. The cavitation intervals used were 0, 15, 30, 45, and 60 minutes. During testing, the materials were dried, and mass loss was recorded with an analytic accuracy of ±0.1 mg. The test results indicate the average of at least three tests per sample.

Microstructural investigation of PM20 and PC20 samples was performed using a scanning electron microscope (SEM) (JEOL JSM-6610LV). For the recording, the carbon coating was applied using the table-top sputter coater LEICA SCD005. The magnification of the equipment ranges from 5 to 300,000 times. The electron source is a W wire (LaB 6). The voltage ranges from 0.3 to 30 kV. The instrument operates on a vacuum system.

An open-source software, JMicroVision v1.3.1.38 [32], was used as an image analysis tool. This software can measure, identify, characterize, and quantify various picture components. It supports extremely large photos and boasts a robust feature set with an easy-to-use interface. Similar to a microscope, it enables dynamic specimen observation with the option to combine several lighting or focus modes (fluorescent, polarized light, etc.). Additionally, images can be viewed simultaneously using the magnifying lens and multi-view tool. Each image has its own zoom coefficient and is maintained in the same center location. Main Features: read images in TIFF, BMP, GIF, JPEG, PNG, and PNM formats; Quantification of components—objects or background; object analysis (size, shape, orientation, texture); image processing (binary and morphology operations, filtering, segmentation); image rectification (geometric corrections by control points); digital point counting; tools for data collection in one or two dimensions; image annotation (variation of granulometry, density, objects, or background).

RESULTS AND DISCUSSION

The mass loss diagram (Fig. 3a) depicts the damage outcomes by plotting the mass loss values on the ordinate and the time of material exposure to the cavitation erosion on the abscissa. Mass loss was measured after each cavitation erosion sequence (i.e., 0, 15, 30, 45, and 60 min). Similarly, the surface degradation level of samples (Fig. 3b) is a correlation between the measured damaged surface and the surface without damage. The development of superficial pits (Fig. 3c) is presented as an interrelation between the estimated number of pits per sample and exposure time (from 15 to 60 min). The mean area of formed pits (Fig. 3b) was estimated from the number of pits using image analysis [32], and the number was correlated to the cavitation exposure duration.

Figure 3.

After 15 minutes of erosion, the sample PM20 lost 2 mg, while the sample PMC20 lost 1.9 mg of its starting mass. The values for both coating samples are comparable. During the following iteration of the cavitation procedure, the measured mass losses were 5.5 mg for the PM20 coating and 3.9 mg for the PC20 coating. After 45 minutes, the following values were obtained: 9.9 mg and 4.5 mg for PM20 and PC20, respectively. The final values of mass loss (60 minutes of water exposure) were 13 mg and 6.9 mg for mullite and corundum-based coatings, respectively. It can be concluded that the mullite-based coating (PM20) was losing mass due to cavitation erosion more rapidly than the PM20 coating.

The level of surface area degradation was estimated for the PM20 and PC20 samples, whose initial surface area was 1257 mm^2. Estimated degraded areas on each sample (PM20 and PC20, respectively) after the cavitation erosion cycle were: 7.2 % and 2.9 % after 15 minutes of exposure; 12.8 % and 4.3 % after 30 minutes of exposure; 14.7 % and 8.1 % after 45 minutes of exposure; and 17.7 % and 8.5 % after 60 minutes of exposure. Even though the percentage of degraded areas is small, it can be noted that the degraded surface progression is more rapid for the mullite-based sample.

The estimated number of pits followed the trend of increasing which is characteristic for the PM20 sample: 98 (after 15 minutes of exposure), 109 (after 30 minutes of exposure), 173 (after 45 minutes of exposure), and 197 (after 60 minutes of exposure). The number of pits was comparatively lower for the PC20 sample for each cavitation exposure sequence: 67 (after 15

minutes), 96 (after 30 minutes), 146 (after 45 minutes), and 129 (after 60 minutes). During the last sequence for the PC20 sample, the number of pits started decreasing. By comparing diagrams Fig. 3b and Fig. 3c, it can be assumed that in the case of PC20 coating, the new pits ceased opening after 45 minutes, while the existing pits started widening or merging.

Upon estimating the degraded area, but taking in account only area under pits, the following results are acquired: 2 mm^2 after 15 minutes of exposure, 2.25 mm^2 after 30 minutes of exposure, 2.4 mm^2 after 45 minutes of exposure, and 2.65 mm^2 after 60 minutes of exposure for the PM20 sample; and 0.9 mm^2 after 15 minutes of exposure, 1.1 mm^2 after 30 minutes of exposure, 1.3 mm^2 after 45 minutes of exposure, and 1.4 mm^2 after 60 minutes of exposure for the PC20 sample. The area under pits was smaller for the corundum-based coating.

The corundum-based coating is more resistant to cavitation erosion than the mullite-based coating, probably due to the difference in the filler's Mohs hardness. Namely, pure mullite mineral is 6-7 on the Mohs hardness scale, while corundum is 9.

The rate of cavitation is calculated from the measured mass loss for each testing period. The points of the diagram are approximated by a straight line using the least squares method. The tangent of the slope depicts the loss of mass during the period of cavitation activity and represents the rate of cavitation erosion. For each set of tested samples, three samples were used, and the findings represent the mean value of these measurements for each test interval. The cavitation rate given in Fig. 4 is a quantifiable measurement of the intensity of material degradation caused by cavitation.

Based on the determined cavitation velocity values, the resistance to the cavitation effect of the investigated samples can also be assessed. Namely, the cavitation rate for the PM20 sample is v = 0.22 mg/min, while the obtained value for the PC20 sample is lower: v = 0.14 mg/min. This means that corundum-based coating is less rapidly deteriorating than mullite-based coating.

Figure 4.

Figure 5.

Figure 5 shows the surfaces of the coating samples during the cavitation erosion test (0–60 minutes) with the corresponding profile lines obtained by image analysis.

The profile lines of the PM20 and PC20 refractory coatings are uniform up to 45 minutes of exposure. Individual peaks, which are present on the profile-line diagram, refer to the presence of singular pits on the surface of each sample. A certain number of pits were identified on the original PM20 and PC20 samples (prior to cavitation erosion testing). In the case of the PM20 sample, larger peaks are observed on the profile line for 60 minutes of cavitation in comparison with the corresponding profile line for the PC20 sample. The formation and development of the damage to the surface of the exposed samples took place at a low speed. The results presented in Fig.4 are in agreement with results provided in Fig.3 a-d.

Figures 6 and 7 show SEM microphotographs of the characteristic eroded surfaces of the coatings PM20 and PC20 created during testing the effect of cavitation.

Figure 6.

Figure 7.

The initial untreated coatings PM20 (Fig. 6) and PC20 (Fig. 7), as seen in the SEM microphotographs on the left side (a, c, and e), show filler particles of various sizes and shapes dispersed uniformly inside the epoxy matrix. The coating applied to the metal substrate is clearly free of defects, bubbles, and delamination. The samples PM20 (Fig. 6) and PC20 (Fig. 7) recorded following the final 60-minute cavitation erosion phase are shown on the right (b, d, and f). The given microphotographs demonstrate that the pits are primarily superficial. There are no void clusters of deeper channels starting from the superficial cavitation pits. The pits appear to be shallow and have smooth surfaces. Thereby, the metal substrate could not be damaged by water stream action due to the presence of the protective coating.

During this research, several potential limitations occurred. Primarily, there was insufficient sample size for statistical measurements. To make meaningful findings from a study, it is critical to have a large enough sample size. The results are more accurate with a larger sample size. Finding important relationships in the data was challenging because the sample size was too small. To guarantee that the sample is regarded as representative of the community and

that the statistical result may be extrapolated to a broader population, statistical tests typically call for a larger sample size. The plan for future research is to repeat the experiment with a larger sample, expand the number of designed coatings, and finally employ a method for analytical modeling (e.g., artificial neural networks) to predict and optimize the behavior and performance of the protective coatings.

CONCLUSIONS

In this study, refractory coatings for metal substrates were successfully made and evaluated for cavitation erosion resistance using an inorganic filler of 80 wt.% (pyrophyllite and mullite, i.e., pyrophyllite and corundum) and a siloxane resin of 15% in their mix-design. The key findings are summarized as follows:

The average grain in the filler mixture is sub-rounded to sub-angular, which is suitable for creating homogeneous coatings. The addition of recycled corundum and/or mullite increased the hardness of the inorganic filler and, thereby, the coating. When applied to a solid surface, the particles of varied grain-sizes contribute to the formation of a homogeneous and durable coating layer. The coatings adhered properly to the metal plate, completely covering the surface and leaving no bumps or bubbles. The coating dried quickly in the air and exhibited no delamination or defects.

The monitoring of mass loss during cavitation erosion tests allowed for the assessment of the cavitation rate. The cavitation rates of 0.22 mg/min and 0.14 mg/min for PM20 and PC20 coatings, respectively, suggest that both coatings deteriorated relatively slowly. The corundum-based coating is more resistant to cavitation erosion than the mullite-based coating, probably due to the difference in the filler's Mohs hardness.

The morphology of the PM20 and PC20 coatings during the final 60-minute cavitation erosion phase exhibited mostly superficial pits. There are no vacant clusters of deeper channels starting from the surface cavitation pits. The coating layer protected the metal substrate from damage caused by an intense water stream.

This study demonstrates that the investigated coatings based on pyrophyllite and waste raw materials can be implemented in conditions that involve substantial cavitation loads while still providing adequate protection for the substrate.

ACKNOWLEDGEMENTS

This work was supported by the Ministry of Science, Technological Development and Innovation of the Republic of Serbia (Contracts No.: 451-03-66/2024-03/200213, 451-03-66/2024-03/ 200012 and 451-03-65/2024-03/200135).

REFERENCES

1. Global Status Report for Buildings and Construction: https://www.unep.org/resources/publication/2022-global-status-report-buildings-and-construction (accessed on 02.02.2024)
2. S. Dora, K.M. Mini, J. Energy Storage 72 (2023) 108550. https://doi.org/10.1016/j.est.2023.108550
3. A. Liebringshausen, P. Eversmann, A. Göbert, J. Build. Engin. 80 (2023) 107696. https://doi.org/10.1016/j.jobe.2023.107696
4. Y. Ettahiri, D. M. Samuel, L. Bouna, A. Khali, A. Aziz, A. Benlhachemi, L. Pérez-Villarejo, W. Kriven, J. Build. Eng. 80 (2023) 108021. https://doi.org/10.1016/j.jobe.2023.108021
5. Y. Ettahiri, L.n Bouna, J. Hanna, A. Benlhachemi, H. L. Pilsworth, A. Bouddouch, B. Bakiz, Mater.s Chem. Physics 296 (2023) 127281. https://doi.org/10.1016/j.matchemphys.2022.127281
6. A.P. Galvín, S. Sabrina, B. Auxi, A. Peña, A. López-Uceda, J. Environ. Manage. 344 (2023) 118409. https://doi.org/10.1016/j.jenvman.2023.118409
7. E. Marsh, J. Orr, T. Ibell, Energy Build. 251 (2021) 111340. https://doi.org/10.1016/j.enbuild.2021.111340
8. S. Mohammadnejad, J. Provis, J. van Deventer, Hydrometallurgy 146 (2014) 154-163. https://doi.org/10.1016/j.hydromet.2014.04.007
9. R. Wardle, G.W. Brindley, Am. Mineral. 57 (1972) 732 -750 (https://rruff.geo.arizona.edu/doclib/am/vol57/AM57_732.pdf, accessed 03.04.2024)
10. J. Temuujin, K. Okada, T. Jadambaa, K. MacKenzie, J. Amarsana, J. Eur. Ceram. Soc. 23 (2003) 1277-1282, https://doi.org/10.1016/S0955-2219(02)00297-2.
11. C. Maqueda, J.L.P. Rodríguez, A. Justo, Analyst 112 (1987) 1085-1086. https://doi.org/10.1039/AN9871201085

12. Y. Ettahiri, L. Bouna, A. Brahim, A. Benlhachemi, B. Bakiz, P. Sánchez-Soto, D. Eliche-Quesada, L.Pérez-Villarejo, Appl. Mater. Today 36 (2024) 102048. https://doi.org/10.1016/j.apmt.2023.102048
13. K. Zhao, W. Yana, X. Wang, B. Hui, G. Gu, H. Wang, Int. J. Miner. Process. 161 (2017) 78-82. https://doi.org/10.1016/j.minpro.2017.02.015
14. X. Pan, Z. Shi, C. Shi, T. Ling, N. Li, Constr. Build. Mater. 132 (2017) 578-5910. https://doi.org/10.1016/j.conbuildmat.2016.12.025
15. L. Bouna, A. Ait El Fakir, Y. Ettahiri, H. Abara, A. Jada, K. Draoui, A. Benlhachemi, M. Ezahri, Mater. Chem. Physics 314 (2024) 128858. https://doi.org/10.1016/j.matchemphys.2023.128858
16. X. Lu, L. Wang, C. Chen, J. Chen, J. Zhou, J. Deng, Constr. Build. Mater. 400 (2023) 132849 https://doi.org/10.1016/j.conbuildmat.2023.132849
17. J.B. Aguiar, C. Júnior, Constr. Build. Mater. 49 (2013) 478-483. https://doi.org/10.1016/j.conbuildmat.2013.08.058
18. M. Shariatmadar, P. Gholamhosseini, Z. Abdorrezaee, S. Ghorbanzadeh, S. Feizollahi, F.S. Hosseini, F. Azad Shahraki, M. Mahdavian, Surf. Coat. Technol. (2024) 130501 https://doi.org/10.1016/j.surfcoat.2024.130501
19. X. Liu, Prog. Org. Coat. 149 (2020) 105892 https://doi.org/10.1016/j.porgcoat.2020.105892
20. H. Qu, M. Feng, M. Li, D. Tian, Y. Zhang, X. Chen, G. Li, Mater. Today Commun. 37 (2023) 107284 https://doi.org/10.1016/j.mtcomm.2023.107284
21. S. Gu, H. Shi, J. Li, H. Xu, I. I. Udoh, F. Liu, E. Han, Prog. Org. Coat. 183 (2023) 107789 https://doi.org/10.1016/j.porgcoat.2023.107789
22. F. Sun, J. Fu, Y. Peng, X. Jiao, H. Liu, F. Du, Y. Zhang, Prog. Org. Coat. 154 (2021) 106187 https://doi.org/10.1016/j.porgcoat.2021.106187
23. S.A.T. Nejad, S. Amanian, E. Alibakhshi, M. Hajisoltani, S.A. Haddadi, M. Arjmand, B. Ramezanzadeh, M. Mahdavian, Prog. Org. Coat. 188 (2024) 108195. https://doi.org/10.1016/j.porgcoat.2023.108195
24. W. Merks, Clausthal-Zellerfeld, Germany, (1985). (https://search.worldcat.org/title/607758613, accessed on 03.04.202421
25. J. Santamarina, G. Cho,Soil Behavior: The Role of Particle Shape. Conference on Advances in Geotechnical Engineering, London, 29-31 (2004) 604-617.

https://doi.org/10.1061/40659(2003)2
26. . Z. Hossain, I.L. Fabricius, H.F. Christensen, Leading Edge 28 (2009) 86–88. https://doi.org/10.1190/1.3064151
27. A. Terzić, D. Radulović, M. Pezo, J. Stojanović, L. Pezo, Z. Radojević, Lj. Andrić, Constr. Build. Mater. 258 (2020) 119721. https://doi.org/10.1016/j.conbuildmat.2020.119721
28. M. Pavlović, M. Dojčinović, M. Harbinja, A. Hođić, M. Stojanović, Z. Čeganjac, Z.Aćimović, Struct. Integ. Life 23:3 (2023) 257-260. (http://divk.inovacionicentar.rs/ivk/ivk23/OF2303-5s.html, accessed on 03.04.2024.)
29. M. Pavlović, M. Dojčinović, M. Harbinja, A. Hođić, D. Radulović, M. Stojanović, Z. Aćimović,in Proceedings of the 54th International October Conference on Mining and Metallurgy (2023) 357-360. (https://ioc.tfbor.bg.ac.rs/public/2023/Proceedings_IOC_2023.pdf, accessed on 03.04.2024)
30. M. Pavlović, M. Dojčinović: Kavitaciona oštećenja refrakcionih materijala, Akademska misao, Belgrade, (2020), p.165. ISBN 978-86-7466-823-8. (https://akademska-misao.rs/product/kavitaciona-ostecenja-vatrostalnih-materijala/ accessed on 01.03.2024)
31. ASTM G32-16 Red Standard Test Method for Cavitation Erosion Using Vibratory Apparatus (Standard + Redline PDF Bundle), https://webstore.ansi.org/standards/astm/astmg3216red (accessed 15.03.2024).
32. Jmicro Vision program: https://jmicrovision.github.io/(accessed 15.03.2024).

Figures

Figure 5. PM20 and PC20 coating samples exposed to cavitation test with accompanying profile lines.

Figure 6. SEM microphotographs of the PM20 coatings: a), c), and e) prior to cavitation; and b), d), and f) after 60 min of cavitation.

Figure 7. SEM microphotographs of the PC20 coatings: a), c), and e) prior to cavitation; and b), d), and f) after 60 min of cavitation.

Table 1. Quantification of the major oxides in mineral raw materials used for filler preparation.

Oxide, %	SiO_2	Al_2O_3	Fe_2O_3	CaO	MgO	K_2O	Na_2O	TiO_2	SO_3	LoI*
Pyrophyllite	68.30	16.20	1.49	6.27	1.14	0.61	0.38	0.15	0.01	5.45
Mullite	13.81	83.14	0.32	-	-	-	-	-	-	2.73
Corundum	2.59	95.80	0.10	-	-	-	-	-	-	1.51

* Loss on ignition at 1000 °C

Table 2. Mix-design of the coatings.

Sample	Mullite (%)	Corundum (%)	Pyrophyllite (%)	Siloxane resin (%)	Coupling agent (%)	Titanium dioxide (%)
PM20	20	-	80	15*	3.5*	1.5*
PC20	-	20	80	15*	3.5*	1.5*

* Of the total mass

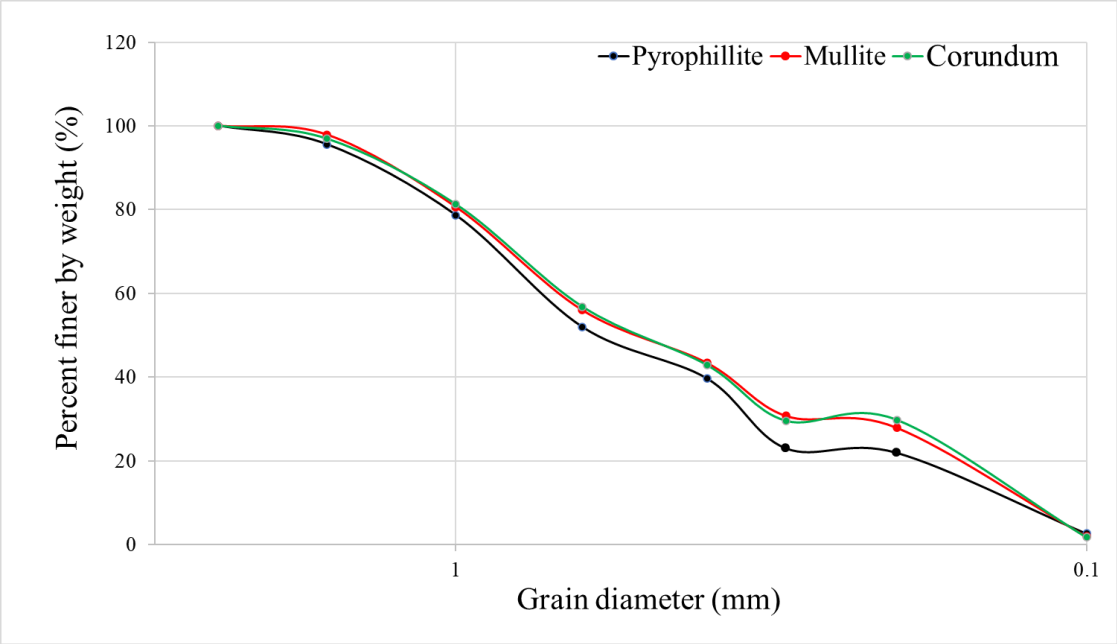

Figure 1

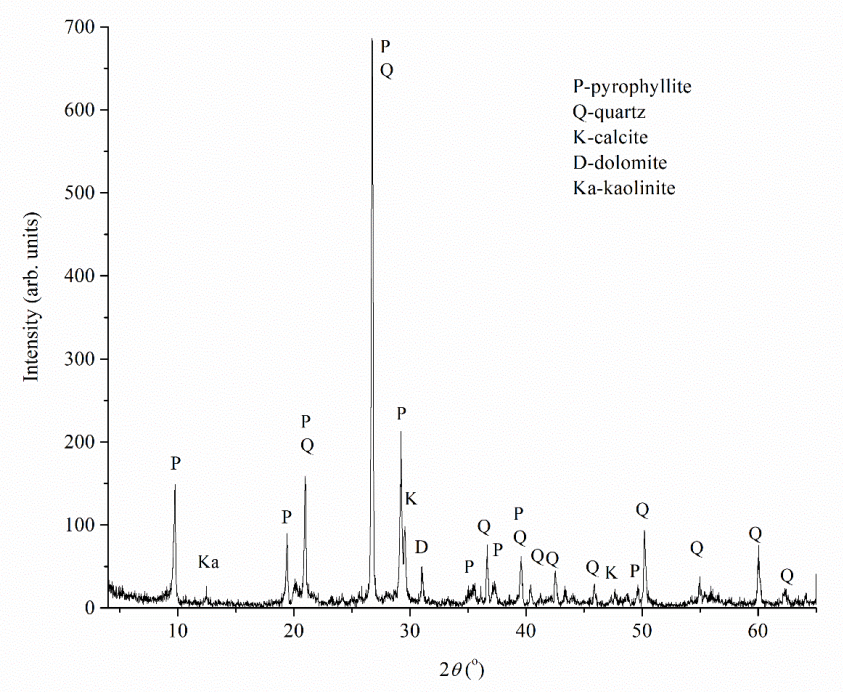

Figure 2

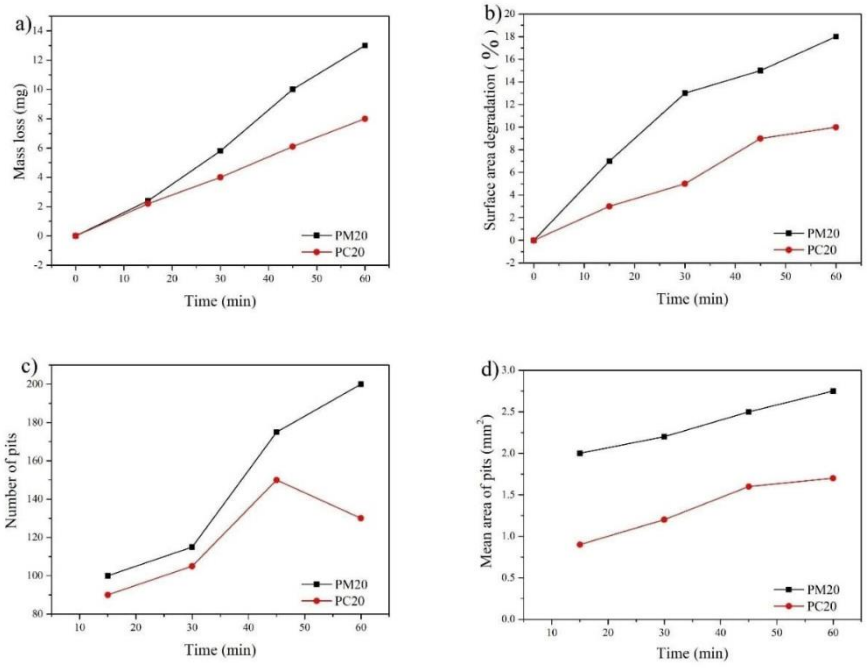
a)
Mass loss (mg)
Time (min)
PM20
PC20
b)
Surface area degradation (%)
Time (min)
PM20
PC20
c)
Number of pits
Time (min)
PM20
PC20
d)
Mean area of pits (mm²)
Time (min)
PM20
PC20

Figure 3

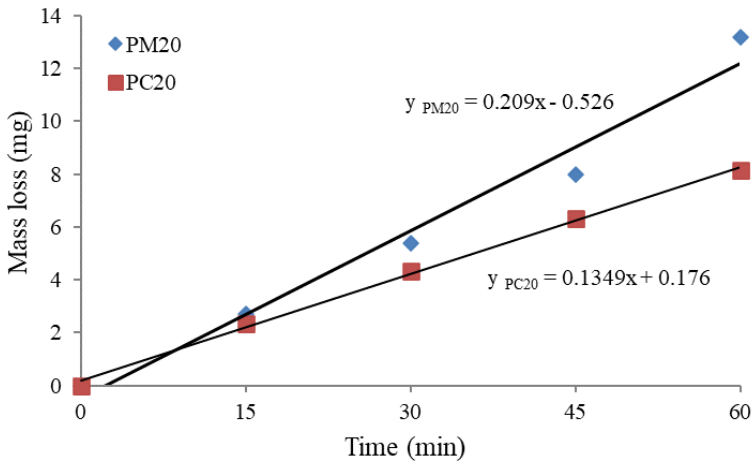
PM20
PC20
y PM20 = 0.209x - 0.526
y PC20 = 0.1349x + 0.176
Mass loss (mg)
Time (min)
0
2
4
6
8
10
12
14
0
15
30
45
60

Figure 4

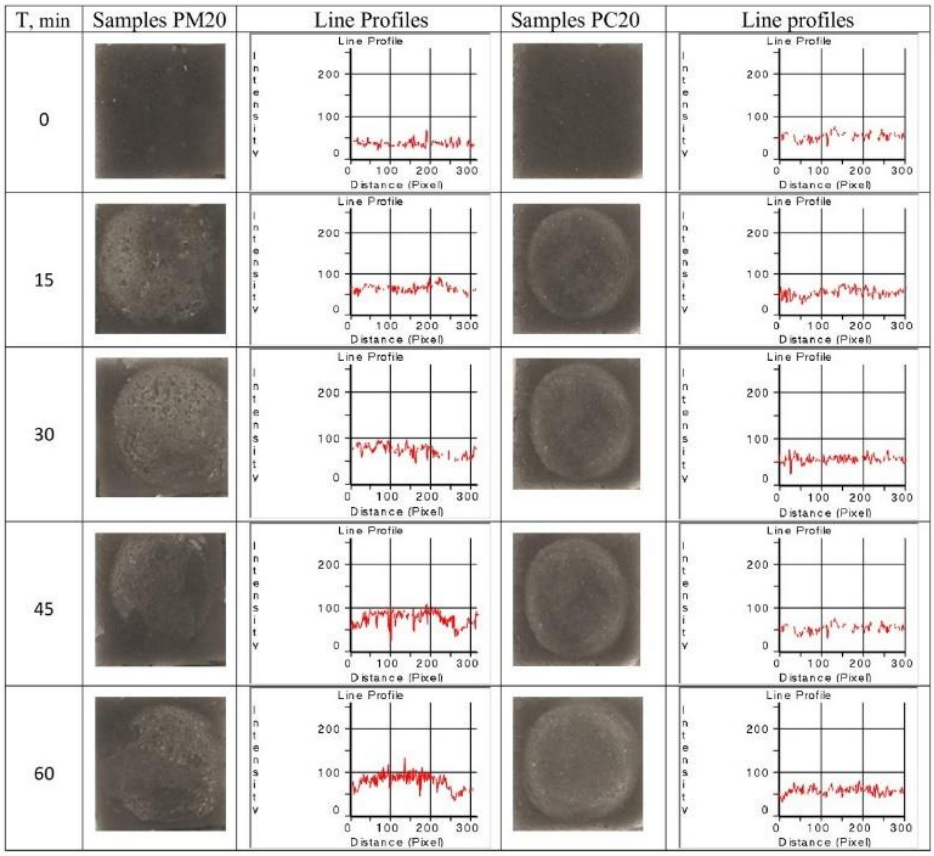
T, min
Samples PM20
Line Profiles
Samples PC20
Line profiles
0
15
30
45
60
Line Profile
Intensity
Distance (Pixel)
0
100
200
300

Figure 5

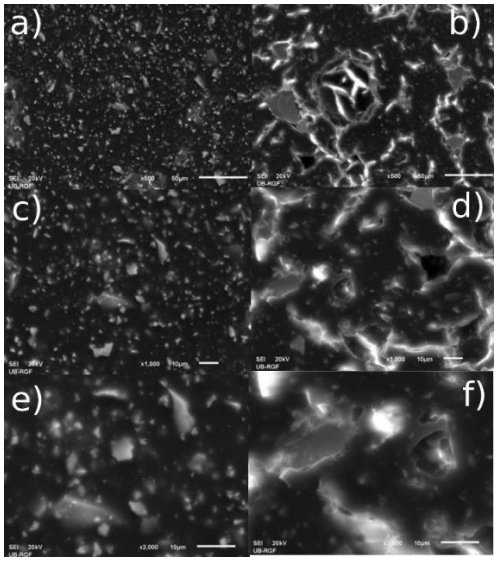

Figure 6

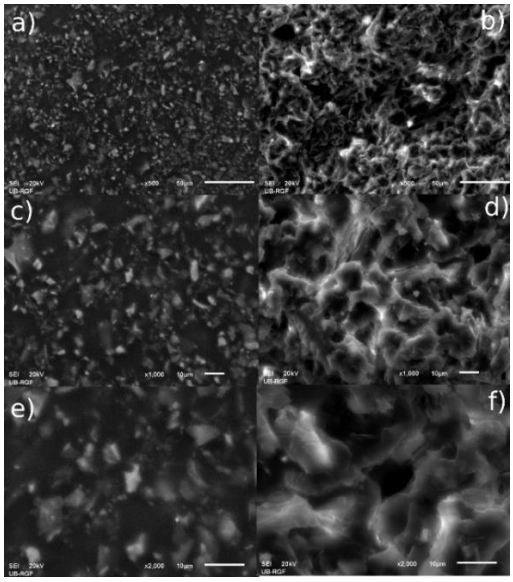

Figure 7